Level scheme study of ^{92}Mo: Searching for the evidence of core-excitation

Z. Huang,[1,2] G. X. Zhang,[3,2,4,*] G. L. Zhang,[1,†] S. P. Hu,[5] S. M. Lenzi,[2,4] D. Mengoni,[2,4] J. L. Ferreira,[6] Y. F. Lv,[7] J. B. Lu,[7] B. Paes,[6] E. N. Cardozo,[6] H. Q. Zhang,[8] H. B. Sun,[9] J. J. Valiente-Dobón,[10] D. Testov,[2,4] A. Goasduff,[10] D. Bazzacco,[2,4] P. R. John,[11] D. R. Napoli,[10] F. Galtarossa,[10] F. Recchia,[10] G. de. Angelis,[10] M. Siciliano,[10,12] R. Menegazzo,[10] and J. Lubian[6]

[1] *School of Physics, Beihang University, Beijing 100191, China*
[2] *Dipartimento di fisica Astronomia dell'Universita di padova, Padova, Italy*
[3] *Sino-French Institute of Nuclear Engineering and Technology, Sun Yat-sen University, Zhuhai 519082, Guangdong, China*
[4] *Istituto Nazionale di Fisica Nucleare, Sezione di Padova, Padova, Italy*
[5] *Institute for Advanced Study in Nuclear Energy, Shenzhen University, Shenzhen 518060, China*
[6] *Instituto de Física, Universidade Federal Fluminense, 24210-340, Niterói, Rio de Janeiro, Brazil*
[7] *College of Physics, Jilin University, Changchun 130012, China*
[8] *China Institute of Atomic Energy, Beijing 102413, China*
[9] *College of Physics and Energy, Shenzhen University, Shenzhen 518060, China*
[10] *INFN, Laboratori Nazionali di Legnaro, I-35020 Legnaro, Italy*
[11] *Institut für Kernphysik der Technischen Universität Darmstadt, Germany*
[12] *Physics Division, Argonne National Laboratory, Lemont-IL, USA*

(Dated: December 19, 2022)

Excited states in ^{92}Mo are populated via the ^{89}Y(^{6}Li, $3n$)^{92}Mo reaction at the tandem of XTU, INFN-LNL. Level scheme of ^{92}Mo is revised and expanded considerably by the γ-γ coincidence measurement. The newly observed level structures are compared with different shell-model calculations performed in various model spaces. The results show that the several high-energy ($\sim$ 2 MeV) transitions, observed for the first time in the current work, could be a presumable signature of $N = 50$ core-breaking effect. The measured strengths of $E1$ transitions between the low-lying positive and negative bands indicate an importance contribution from $Z = 28$ proton core-excitation.

I. INTRODUCTION

In last decades, the level structures of semi-magic (N = 50) nuclei have attracted huge amount of attentions from both theoretical and experimental points of view [1]. Particular interests focus on the conservation of seniority quantum number in the low-lying states [2–4] and the Z = N = 50 core-breaking effect in the high-lying states [5–8].

In the previous works [9–14], the understanding of ^{92}Mo level scheme starts from low-lying positive and negative bands built on four-proton configurations within the valence proton space including $\pi(p_{1/2}, g_{9/2})$ orbits (with an inert ^{88}Sr core). For the positive band, the $0_1^+, 2_1^+, 4_1^+, 6_1^+$ and 8_1^+ states can be well described by the mixed proton configurations between $\pi((p_{1/2})^2, (g_{9/2})^2)$ and $\pi((p_{1/2})^0, (g_{9/2})^4)$. The same model space would show a less perfect agreement for states higher than 10_1^+ at 5.1 MeV, due to the fact that the contributions from the deeper bounding $\pi(f_{5/2}, p_{3/2})$ orbits [14] or $Z = N = 50$ core-breaking effect are missing in the current space.

For the low-lying negative states, proton configuration $\pi((p_{1/2})^1, (g_{9/2})^3)$ in the same model space can also accurately characterize $5_1^-, 7_1^-, 9_1^-$ and 11_1^- states. Again this model drastically decreased its prediction power for states higher than 12^- at 6.5 MeV. Being similar with the case of 10_1^+ state, the origins of these high-lying negative states are most likely related to the Z = 38 or $Z = N = 50$ core-excitations because of the significant energy difference between 11_1^- and 12_1^- states (2.064 MeV).

In Ref. [14], Ghugre *et al*. suggest that the excitation of a single proton across the Z = 38 gap could be responsible for $12_1^-, 13_1^-$ states, and the N = 50 across-shell excitation could explain the even-higher states with $I = 15_1^-, 16_1^-, 17_1^-$. However, a discrepancy occurs later in Ref .[15], in which Pattabiraman *et al*. had performed a new measurement using the Clover detector. New result shows that the parities of aforementioned high-lying negative states ($I = 15_1^-, 16_1^-, 17_1^-$ in Ref. [14]) should be changed to positive. This would lead to more questions on these high-lying positive states, such as their configurations and how they could communicate with the other known low-lying positive states. Therefore, more experimental data on ^{92}Mo are needed in order to confirm the existence of core-breaking effect especially in high-lying part.

On the other side, neither the limited model spaces of $\pi(p_{1/2}, g_{9/2})$ with a ^{88}Sr core, nor the expanded one of $\pi\nu(f_{5/2}, p_{3/2}, p_{1/2}, g_{9/2})$ with a ^{56}Ni core, can explain the existence of $E1$ transition between the negative band and the positive band in ^{92}Mo. This is because the matrix elements $< f|E1|i >$ vanish for all possible combinations of initial states i and final states f in both model

* E-mail address: guangxin.zhang@pd.infn.it
† E-mail address: zgl@buaa.edu.cn

spaces [6]. This $E1$ strength is of particular importance in constructing the lifetime of their initial states and the branching ratios. Up to now, for the semi-magic nucleus with $N = 50$, the $E1$ transition has only been studied in one case of ^{94}Ru [6] by a larger model space, i.e., including $d_{5/2}$ and $g_{7/2}$ orbits above $N = Z = 50$ shell. However, the explanation is still qualitatively, since only the particle excitations from $f_{5/2}p_{3/2}p_{1/2}$ to $g_{9/2}$ orbits as well as $g_{9/2}$ to $g_{7/2}d_{5/2}$ orbits were allowed in this model due to the huge dimension. Thus, more experimental data of $E1$ transition in this semi-magic ($N = 50$) nuclei are desired to compare with more advanced theoretical calculations.

The paper is organized as follows. The experimental setup is shown in Sec. II. Sec. III presents the experimental data analysis and results. The shell model calculation results are discussed in Sec. IV and a summary of the current work is finally given in Sec. V.

II. EXPERIMENTAL SETUP

In order to study the level structure of ^{92}Mo, a ^{6}Li+^{89}Y experiment was performed at INFN-LNL, Italy. A ^{6}Li^{3+} beam with an average intensity of 1.0 enA was speeded up to 34 MeV by the Tandem-XTU accelerator and hit on an ^{89}Y target with a thickness of 550 μg/cm^2. A ^{12}C foil with a thickness of 340 μg/cm^2 backed on the ^{89}Y target was used to stop all the fusion residues. The main products from the fusion of ^{6}Li+^{89}Y system include ^{92}Mo, which is related to the 3n evaporation channel from the compound nucleus ^{95}Mo.

The γ rays emitted from the residues were measured by the GALILEO array [16], which is consisted of 25 Compton-suppressed high-purity germanium detectors. Eight BGO crystals were served as the anti-Compton shield of each detector. All the 25 detectors were put 235 mm away from the target position. Ten of them were placed in a ring of 90° with respect to the beam direction, and other fifteen detectors were mounted at other three rings at 119° (5 detectors), 129° (5 detectors) and 152° (5 detectors), respectively. The typical energy resolution of GALILEO array was measured to be 0.17% for 1332-keV γ ray emitted from ^{60}Co source (FWHM = 2.3 keV). The efficiency for each detector was calibrated by sources with known radioactivity, including ^{60}Co, ^{133}Ba, ^{152}Eu, ^{88}Y, and ^{241}Am, placed at the target position. The full-energy-peak efficiency was measured 2.5% for 1 MeV γ-ray in the current configuration. A 4π Si-ball detector array, named EUCLIDES [17], was placed in the center of GALILEO array to measure the light charged particles produced in the experiment. The charge-particle-γ coincidence measurement enabled the investigation of the level scheme for weakly populated residues. In the current paper, the EUCLIDES data was not used since ^{92}Mo related to the 3n evaporation channel, as mentioned before. The detailed experimental setup can be found in our previous publication [18, 19].

The digital data acquisition system of the GALILEO array is based on the XDAQ framework [20, 21] and different digitizers are synchronized by a distributed clock using Global Trigger System (GTS) with a frequency of 100 MHz, giving a common absolute time (timestamp) with 10 ns resolution for each γ ray by using leading-edge algorithm. In the off-line analysis, time information coming from the Constant Fraction Discriminator (CFD) algorithm is also taken into account [22] in order to get better time resolution as well as compensate the time-walk effect induced by the leading-edge method. Details on the digital data acquisition and electronic modules can be found in Ref. [16].

III. DATA ANALYSIS AND RESULTS

The partial level scheme of ^{92}Mo established in the current work is shown in Fig. 1. In addition to the confirmation of previously known states in Refs. [12, 13, 15, 23–25], fourteen new states and twenty-six new transitions are added in the level scheme of ^{92}Mo for the first time (marked as red levels and red arrows in Fig. 1) based on the γ-γ coincidence analysis.

In order to investigate the level structure of ^{92}Mo, which has an isomeric state ($T_{1/2} = 190 \pm 3$ ns) at $E_x =$ 2760 keV with J^π=8^+_1[26], a prompt-delayed coincidence matrix was generated with prompt γ rays on one axis and delayed γ rays on the other. Figures 2 (a) and (b) show the different energy regions of the γ-ray spectra with summing coincidence gates on 1509.8 keV + 773.0 keV + 329.5 keV γ rays by a delayed time window of 100-500 ns. Most of the newly observed transitions in the current work on top of the J^π=8^+_1 isomer can be clearly identified (marked with red asterisk). Another coincidence γ-ray spectra with a prompt summing gates (time window: ±60 ns) on 234.9 keV + 111.0 keV + 649.5 keV transitions are displayed in Figs. 2 (c) and (d) for different energy regions, in order to highlight the newly observed weak transitions which mainly feed the previous known negative band. Figure 2 (e) shows the γ-ray spectrum with a prompt (time window: ±60 ns) summing coincidence gates on 656.5 keV + 304.2 keV transitions, emphasizing the identification of 2490.4-656.5-304.2 keV cascade. The detailed γ-γ coincidence relationships as well as the relative intensities information are employed to fix the positions for the newly-observed transitions.

In order to characterize the spin of each level, especially for the newly observed ones, the γ-ray angular distribution from the oriented nuclei (ADO) ratio method [27] was used in the current work. Assuming a γ_1 - γ_2 cascade exists in one nucleus, the ADO ratio of γ_1 in the current experimental setup can be defined as:

$$R_{ADO}(\gamma_1) = \frac{I_{\gamma_1} \text{at } 152^\circ, \text{ gated with } \gamma_2 \text{ at any angles}}{I_{\gamma_1} \text{at } 90^\circ, \text{ gated with } \gamma_2 \text{ at any angles}},$$

where I_γ is the γ-ray intensity after efficiency corrections. By evaluating the R_{ADO} values for the γ rays with known

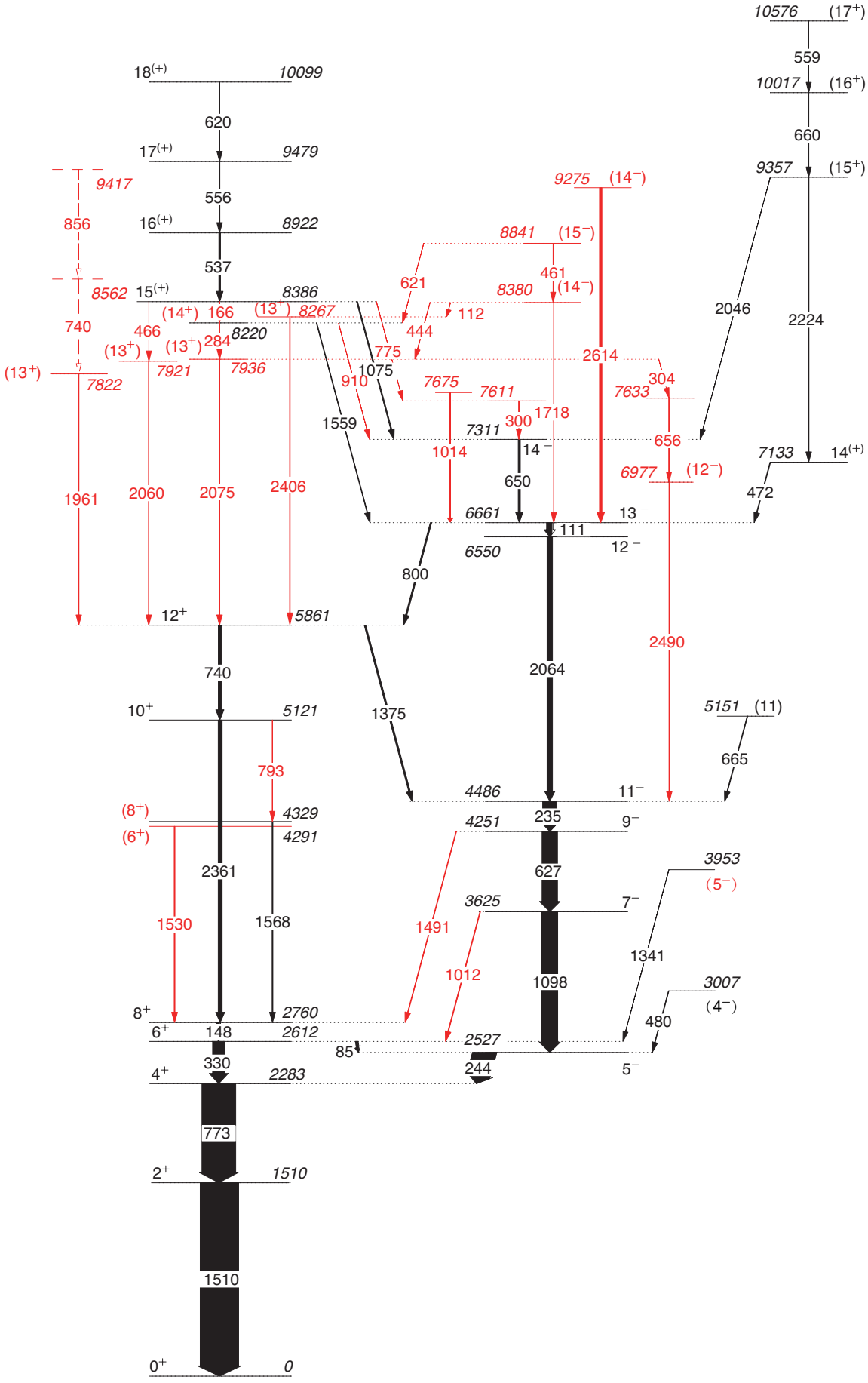

FIG. 1. (Color online) Partial level scheme of ^{92}Mo established in the current work. The newly observed levels and transitions are in red color. The width of the arrows indicates the relative γ-ray intensities. The energies are given in keV units.

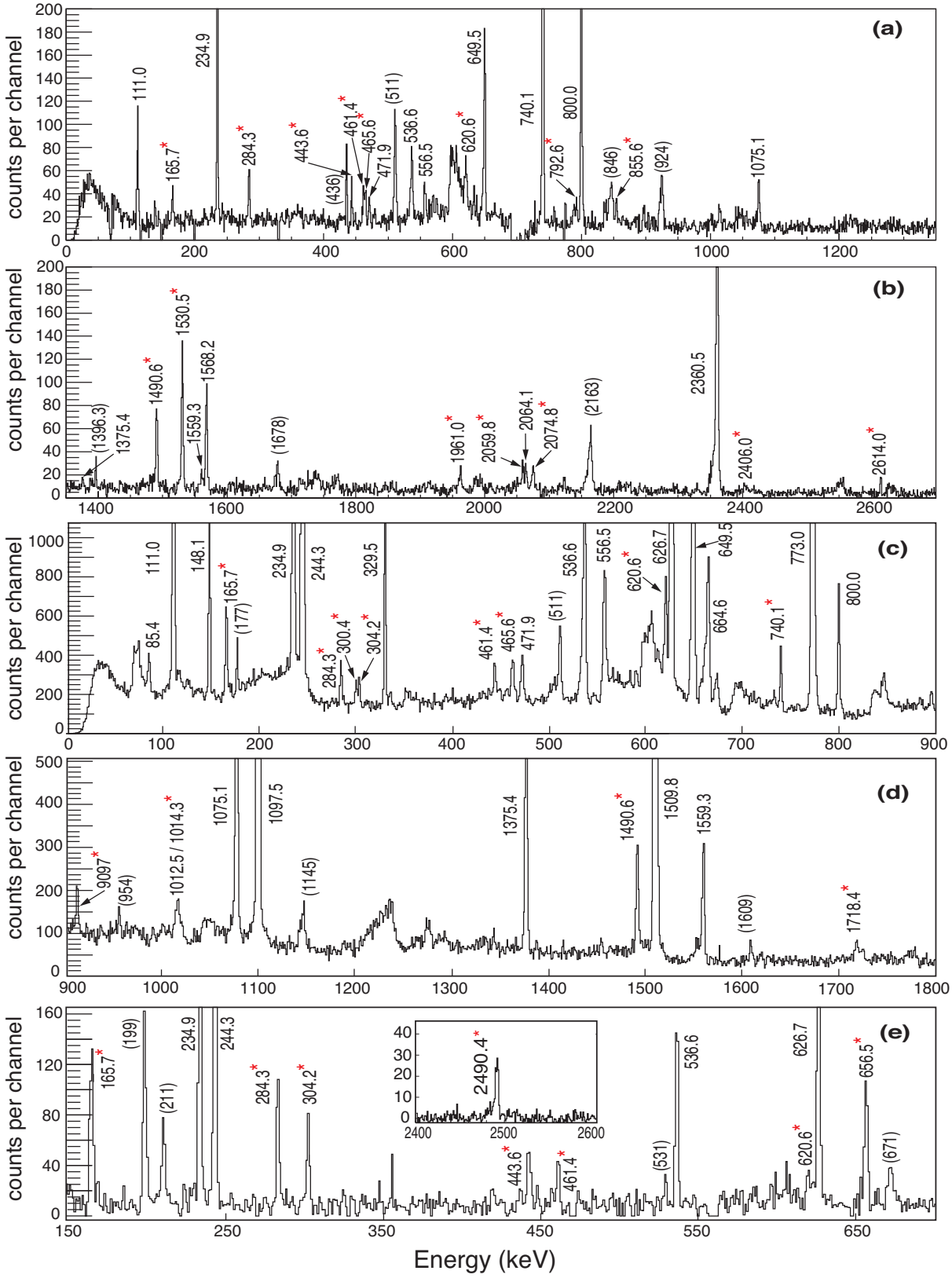

FIG. 2. (a) and (b): Coincidence spectra from the sum of delayed (time window: 100-500 ns) gates on 1509.8 keV + 773.0 keV + 329.5 keV γ-rays. (c) and (d) Prompt (time window: $\pm$60 ns) γ-ray coincidence spectra with a summing gates on 234.9 keV + 111.0 keV +649.5 keV γ-rays. (e) Prompt (time window: $\pm$60 ns) γ-ray coincidence spectra with a summing gates on 304.2 keV + 656.5 keV transitions, the inset highlights the newly found 2490.4 keV γ ray. All the new transitions are labeled with asterisk(*), and peaks with parentheses are contamination.

multi-polarity in ^{91,92}Mo, ^{92}Nb, ^{89}Zr produced in the current experiment as shown in Fig .3, it is observed that the R_{ADO} ∼1.6 and ∼0.8 for the stretched quadrupole and the stretched dipole transitions in the current experimental setup, respectively. It should be mentioned that ΔJ = 0 dipole transition has quite similar angular distribution with that of stretched quadrupole transition, giving rise to a comparable R_{ADO} value. The results of R_{ADO} value for new transitions in ^{92}Mo are also shown in Fig .3 with red points, while for some weak transitions it is not obtained due to the limited statistics. Furthermore, since a lack of polarization measurement in the present work, which is crucial to determine the electric or magnetic nature of the transition, the assignment of spin-parity for the newly observed states is still tentatively.

As a short conclusion, the information on γ-ray identified in ^{92}Mo during the current work, including energies, intensities, *ADO* ratios, and spin-parity information of the initial and final states are summarized in Table I.

Lifetime longer than few nano-seconds in ^{92}Mo is also remeasured in this experiment. Due to the fact that the time resolution of GALILEO array was measured to be ≈10 ns using ^{60}Co source, for lifetimes shorter than or close to 10 ns, the centroid difference method was used. The centroid difference method has been well developed in Ref. [28, 29] mainly for the lifetime measurement in pico-seconds region with $LaBr_3$(Ce) scintillation detector. It is of particular importance to determine the prompt response difference (PRD) coming from the time walk effect of both feeding and decay transition using standard source data. As mentioned at the end of last section, the time-walk effect induced by leading-edge method in the data acquisition part is mainly compensated by adding a time information coming from CFD algorithm in the offline analysis to the common time-stamp information (details information can be found in Ref. [22]). As a result, the PRD curve measured by ^{152}Eu source with known lifetime is shown in Fig .4, in which the transitions with energy larger than 200-keV are almost free of time-walk effect, giving residuals smaller than ±1 ns. The weighted average of absolute values of PRD residuals with energies higher than 200-keV is calculated to be 0.458 ns, giving a systematical error of 0.5 ns in the current work.

Considering the experimental result, the 2_1^+ state in ^{92}Mo with lifetime of 0.35(2) ps [26] can be viewed as a prompt case and served as a reference. The delayed and anti-delayed time distributions between the 1510-keV and 773-keV transitions (see Fig. 1 for the position of transitions) are plotted in Fig. 5 (a), which is completely overlapped with each other. Figure 5 (b) presents the delayed and anti-delayed time distributions between the 1098-keV and 244-keV transitions. Thus the lifetime of 5^- state is measured to be 1.8(±0.1±0.5) ns. Here, 0.1 ns and 0.5 ns are statistical error and systematical error, respectively. Similarly, the delayed and anti-delayed time distributions between 1375-keV and 235-keV transitions were used to extract the lifetime of 11^- state, 12.1(±0.8±0.5) ns, shown in Fig. 5 (c). Figure 5 (d) also shows the time-difference spectrum between the γ rays depopulating (148 keV) and feeding (1568 keV and 2361 keV) 8_1^+ state in ^{92}Mo, and by fitting the decay curve a life-time of 281(34) ns is obtained. All the life-times remeasured in the current work are in consistent with the adopted values in NNDC[26].

IV. SHELL MODEL CALCULATIONS AND DISCUSSION

Following the experimental findings presented in this work, we have performed two shell-model calculations with the KSHELL [30] code in order to further illuminate the structure of ^{92}Mo. The JUN45 calculation is performed in the $\pi\nu(p_{3/2}, f_{5/2}, p_{1/2}, g_{9/2})$ model spaces (with a ^{56}Ni core), in which the interaction is firstly obtained with a realistic one based on the Bonn-C potential and then modified empirically in order to reproduce around 400 experimental levels of 69 nuclei with mass numbers A=63∼96 [31]. Another calculation, called JJ-GLEM, is using a larger model space, including $\pi(f_{7/2}, f_{5/2}, p_{3/2}, p_{1/2}, g_{9/2})$ and $\nu(g_{9/2}, g_{7/2}, d_{5/2}, d_{3/2}, s_{1/2})$ orbits. Here all the single-particle energies are taken from Refs. [32, 33], except for the $f_{7/2}$ proton one which is set to be -15.7 MeV. The two-body matrix elements are initially derived from a G-matrix interaction [34] and then fitted in order to achieve a better description for the level scheme of nuclei in the $A = 95 \sim 97$ region. Due to the fact that the JJGLEM model space is too large for the computational capacity, only one proton is permitted to be excited from the $f_{7/2}$ orbit to higher ones, and all neutrons are constrained in $g_{9/2}$ orbit for the current ^{92}Mo case. The details of the JJGLEM calculation can be found in our previous publication [35].

The selected experimental levels are compared with two different theoretical predictions in Fig. 6. In this section, the discussions firstly focus on the positive and negative band mainly based on the comparison between the experimental result and JUN45 calculation. Special attention is given to the $E1$ transition in the last subsection. It should be mentioned that JJGLEM model space could be affected by center-of-mass spurious [36] components when including $f_{7/2}$ and $g_{9/2}$ orbits at the same time. However, the effect of center-of-mass motion on the description of level scheme is still not clear so far. In this work, the JJGLEM calculation is employed mainly to check how much the $Z = 28$ core-breaking (or exciting proton from $f_{7/2}$ orbit) can contribute to the observed $E1$ transition strengths.

A. positive states

As shown in Fig. 6, the previously known positive band in ^{92}Mo, including 0_1^+, 2_1^+, 4_1^+, 6_1^+, 8_1^+, as well as 10_1^+ and 12_1^+ states, can be fairly de-

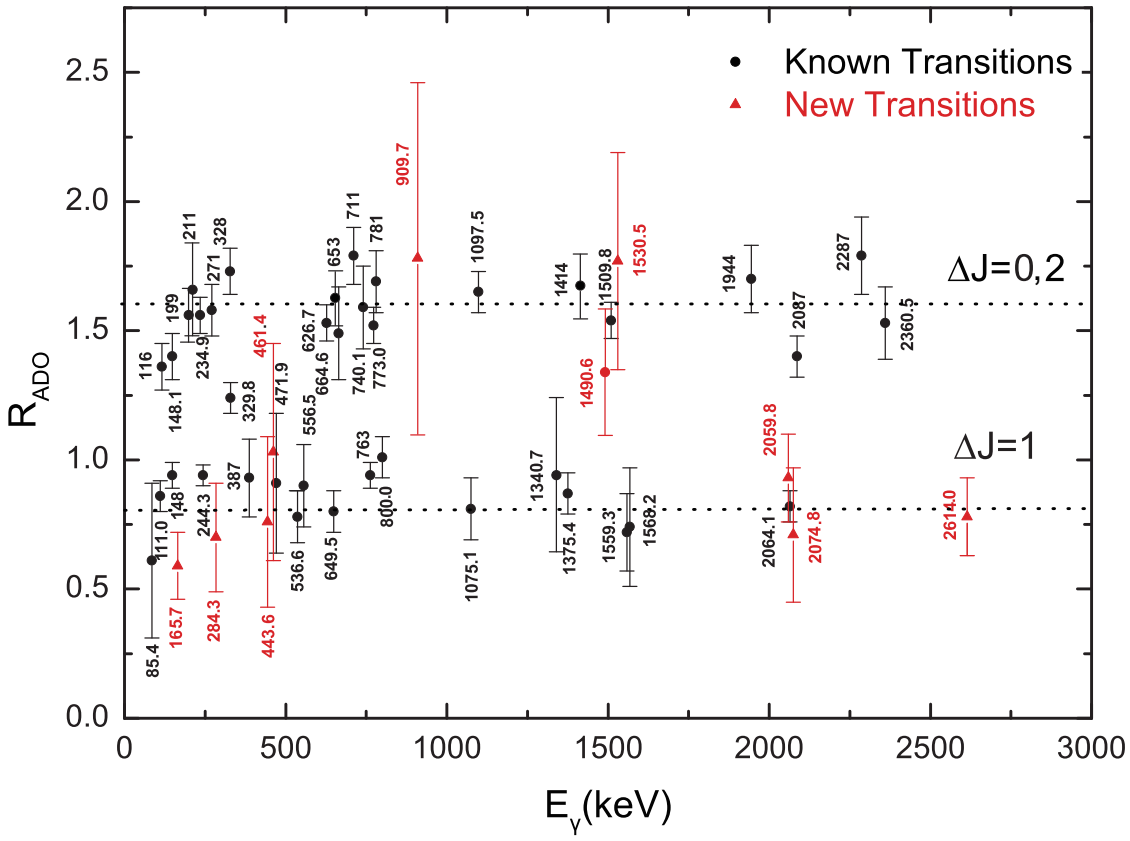

FIG. 3. R_{ADO} plotted for γ-ray transitions of ^{92}Mo. The lines correspond to the value of R_{ADO} for the known quadrupoles and dipoles. The quoted error includes the error due to background subtraction, fitting, and efficiency correction.

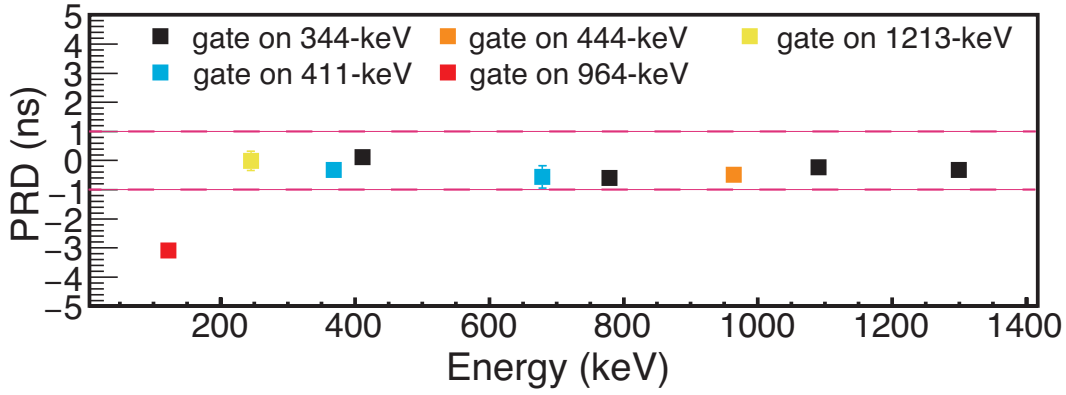

FIG. 4. The prompt response difference (PRD) of GALILEO array measured by ^{152}Eu source.

scribed by the JUN45 calculation. The configurations obtained by JUN45 model are summarized in Table II, in which the aforementioned states are dominated by $\pi((p_{3/2})^4,(f_{5/2})^6,(p_{1/2})^2,(g_{9/2})^2)$ configurations, while the 10_1^+ and 12_1^+ states are dominated by $\pi((p_{3/2})^4,(f_{5/2})^6,(p_{1/2})^0,(g_{9/2})^4)$ configurations. In addition, the configurations involving exciting protons from the $(p_{3/2},f_{5/2})$ shell also contribute significantly ($\approx 10-20\%$) to these states. Here the neutron configuration is omitted since in JUN45 model space they are fully occupied in the ^{92}Mo with $N=50$.

Another two states between 8_1^+ and 10_1^+ are experimentally observed at 4291- and 4329-keV as shown in Fig. 6. For the second one, only one decay transition of 1568-keV transition towards 8_1^+ is known before[24], thus the spin-parity of that state cannot be fixed. In the current work, this 4329-keV state has been tentatively assigned to 8_2^+, due to the facts: (1) a 793-keV transition connecting the 10_1^+ and this state is observed for the first time (see Fig. 1 and Fig. 2(a)), and (2) JUN45 calculation also predicts a second 8^+ between 8_1^+ and 10_1^+ states as shown in Fig. 6. On the other hand, the relative intensity between 793-($10_1^+\rightarrow 8_2^+$) and 2361-keV($10_1^+\rightarrow 8_1^+$) transitions is measured to be 2.3(3) and 100.0(41) experimentally by gating on 740-keV (feed the 10_1^+ state, see Fig. 1) γ ray. This measured branching ratio of 2.0(3)% between the aforementioned two $E2$ transitions is fairly consistent with the value of 3.2% from JUN45 calculation in which the calculated $B(E2)$s (4.4 and 0.8 W.u.) and the transition energies (865- and 2422-keV) are taken into account. The other one at 4291 keV, which is only 38 keV lower than the 8_2^+ state, is observed for the first time. Its spin-parity is tentatively assigned as 6_2^+, since the depopulated 1530-keV transition directly feeds the 8_1^+ state and R_{ADO} ratio (see Fig. 3).

As mentioned in the introduction part, the spin-parities of 8386, 8922 and 9479-keV level are determined to be 15^+, 16^+, 17^+ by a Clover measurement [15], therefore no positive states between 12_1^+ and $15_1^{(+)}$ are previously known in ^{92}Mo. In the current work, two cascades of 466-2060-keV and 166-284-2075-keV transitions (see Fig. 2 (a) and (b)) are newly observed connecting the 12_1^+ and $15_1^{(+)}$ states. The ordering of the transitions in the latter cascade can be unambiguously determined due to the findings of inter-band transitions as shown in Fig. 1. According to the *ADO* ratios of 284-, 2060-, and 2075-keV transitions, (13_2^+), (13_3^+), and (14_1^+) were tentatively assigned to the states at 7921, 7936, and 8220 keV, respectively. Two high-energy γ rays at 1961- and 2406-keV (see Fig. 2 (b)) are also observed for the first time which directly feed the 12_1^+ state, and the spin-parities of their initial states (at 7822 and 8267 keV) are tentatively assigned to be 13^+ (the first and fourth ones as shown in Figs. 1 and 6).

In order to understand the nature of aforementioned high-lying positive band of ^{92}Mo (Z = 42, N=50), we should start from the point that four protons in $p_{1/2},g_{9/2}$ orbits can only give spin up to $12\hbar$ with positive parity. Thus for the states above 12_1^+, the protons excitation over the $Z=38$ sub-shell or neutron excitation across the $N=50$ shell have to be taken into account. This is consistent with the fact that the energy differences between 12^+ and the newly observed (13_1^+), (13_2^+), (13_3^+), (13_4^+) are large ($\sim$ 2000 keV). Meanwhile, as shown in Fig. 6, only one of these four (13^+) states can be characterized by the JUN45 calculation which has a dominant configuration of one proton excitation across the $Z=38$ sub-shell, i.e, $\pi((p_{3/2})^3,(f_{5/2})^6,(p_{1/2})^1,(g_{9/2})^4)$ as listed in Table II. Another calculated 14^+ state with the same configuration might correspond to one of these four measured (13^+) states or to the (14^+) state at 8220-keV. As shown in Table II, the JUN45 calculation includes the second 13^+ and 14^+ states as well. The configuration is dominated by $\pi((p_{3/2})^4,(f_{5/2})^5,(p_{1/2})^1,(g_{9/2})^4)$. However, these states are predicted to be 700–800 keV higher than the yrast one, making it difficult to match any experimental levels.

Anyway, the conclusion is that there are still three among five newly observed states (at 7822, 7921, 7936, 8220, and 8267 keV) which cannot be described within the JUN45 model space. Since all these states decay towards 12_1^+ state directly or indirectly, the remaining states could be attributed to $N=50$ neutron core excitation which is not considered in JUN45 calculation. It should be mentioned that the $N=50$ core-excited state in ^{98}Cd has been measured in Ref. [8] with excitation energy of 6.6 MeV.

Furthermore, the JUN45 calculation significantly overestimates the excitation energy of 15^+ as one can see in Fig. 6. The observed bands built on 15_1^+ (8386 keV) and 15_2^+ (9357 keV) states (see in Fig. 1) show a collective-like structure. This might be another indication of $Z=N=50$ core-breaking effect, giving rise to the emerging and increasing interaction between valence proton and neutron [37]. Anyhow, other theoretical description with larger model space is needed to explain the collective-like structure as well as the possible enhancement of collectivity.

B. negative states

The lowest observed negative-parity state in ^{92}Mo is 5^- which can be formed by aligned coupling between two protons in $p_{1/2}$ and $g_{9/2}$ orbits, and the analog 5^- states can be also observed at similar excitation energies in ^{94}Ru [6], ^{96}Pd [7] and ^{98}Cd [38]. The current JUN45 calculation also predicts 5^- to be the lowest negative-parity state in ^{92}Mo at comparable excitation energy with the experimental result as shown in Fig. 6. The configuration of 5^- state is also predicted to be dominated by $\pi((p_{3/2})^4,(f_{5/2})^6,(p_{1/2})^1,(g_{9/2})^3)$ as listed in Table II and the same one can give maximum spin up to $11\hbar$, reasonably reproduces all the measured $7^-, 9^-$ and 11^- states.

TABLE I. Summary of the energy, relative intensity, ADO ratio, spin-parities for the initial and final states of observed transitions in ^{92}Mo. The new transitions are marked with an asterisk(*), the blank indicates no relative information due to the low statistic in present work. Here, all the intensities come from the singles γ-ray spectrum, and ADO ratios are obtained by coincidence spectra.

E_γ (keV)	I_γ(relative)	R_{ADO}	$J_i^\pi \rightarrow J_f^\pi$
85.4(1)	5.9(2)	0.61(30)	$6^+ \rightarrow 5^-$
111.0(1)	13.9(4)	0.86(6)	$13^- \rightarrow 12^-$
111.9(14)			$(14^-) \rightarrow (13^+)$
148.1(1)	$<41.1(12)^{(a)}$	1.40(9)	$8^+ \rightarrow 6^+$
165.7(1)*	$<12.1(4)^{(b)}$	0.59(13)	$15^{(+)} \rightarrow (14^+)$
234.9(1)	35.0(11)	1.56(7)	$11^- \rightarrow 9^-$
244.3(1)	60.9(18)	0.94(4)	$5^- \rightarrow 4^+$
284.3(1)*	0.80(7)	0.70(21)	$(14^+) \rightarrow (13^+)$
300.4(1)*			
304.2(1)*			
329.8(1)	$<46.7(14)^{(a)}$	1.24(6)	$6^+ \rightarrow 4^+$
443.6(1)*	0.5(1)	0.76(33)	$(14^-) \rightarrow (13^+)$
461.4(3)*	0.60(9)	1.03(42)	$(15^-) \rightarrow (14^-)$
465.6(1)*			$15^{(+)} \rightarrow (13^+)$
471.9(1)	1.6(1)	0.91(27)	$14^{(+)} \rightarrow 13^-$
480.0(1)			$(4^-) \rightarrow 5^-$
536.6(1)	3.8(2)	0.78(10)	$16^{(+)} \rightarrow 15^{(+)}$
556.5(1)	1.6(2)	0.90(16)	$17^{(+)} \rightarrow 16^{(+)}$
559.1(1)			$(17^+) \rightarrow (16^+)$
620.4(1)			$18^{(+)} \rightarrow 17^{(+)}$
620.6(1)*			$(15^-) \rightarrow (14^+)$
626.7(1)	40.0(12)	1.53(7)	$9^- \rightarrow 7^-$
649.5(1)	5.4(1)	0.80(8)	$14^- \rightarrow 13^-$
656.5(2)*			
660.2(1)			$(16^+) \rightarrow (15^+)$
664.6(1)	1.6(1)	1.49(18)	$(11) \rightarrow 11^-$
740.1(1)	$< 7.9(2)^{(c)}$	1.59(16)	$12^+ \rightarrow 10^+$
740.1(2)*			
773.0(1)	$< 91.5(28)^{(c)}$	1.52(7)	$4^+ \rightarrow 2^+$
775.1(2)*			
792.6(1)*	0.4(1)		$10^+ \rightarrow (8^+)$
800.0(1)	3.6(1)	1.01(8)	$13^- \rightarrow 12^+$
855.6(5)*			
909.7(1)*	$< 10.0(3)^{(a)}$	1.78(68)	$(14^+) \rightarrow 14^-$
1012.5(1)*			$7^- \rightarrow 6^+$
1014.3(3)*			
1075.1(1)	2.7(1)	0.81(12)	$15^{(+)} \rightarrow 14^-$
1097.5(1)	41.2(12)	1.65(8)	$7^- \rightarrow 5^-$
1340.7(3)	0.90(4)	0.94(30)	$(5^-) \rightarrow 6^+$
1375.4(1)	6.7(2)	0.87(8)	$12^+ \rightarrow 11^-$
1490.6(1)*	1.4(1)	1.34(25)	$9^- \rightarrow 8^+$
1509.8(1)	100(3)	1.54(7)	$2^+ \rightarrow 0^+$
1530.5(1)*	1.7(1)	1.77(42)	$(6^+) \rightarrow 8^+$
1559.3(1)*	1.4(1)	0.72(16)	$(14^+) \rightarrow 13^-$
1568.2(1)	2.0(1)	0.74(23)	$(8^+) \rightarrow 8^+$
1718.4(1)*			$(14^-) \rightarrow 13^-$
1961.0(1)*	0.9(1)		$(13^+) \rightarrow 12^+$
2046.1(1)			$(15^+) \rightarrow 14^-$
2059.8(1)*	1.0(1)	0.93(17)	$(13^+) \rightarrow 12^+$
2064.1(1)	13.1(4)	0.82(6)	$12^- \rightarrow 11^-$
2074.8(1)*	1.3(1)	0.71(26)	$(13^+) \rightarrow 12^+$
2223.9(3)	1.3(1)		$(15^+) \rightarrow 14^{(+)}$
2360.5(1)	9.6(3)	1.53(14)	$10^+ \rightarrow 8^+$
2406.0(1)*	0.2(1)		$(13^+) \rightarrow 12^+$
2490.4(1)*			$(12^-) \rightarrow 11^-$
2614.0(1)*	6.3(2)	0.78(15)	$(14^-) \rightarrow 13^-$

(a) Gamma rays exist in both ^{92}Mo and ^{92}Nb.
(b) Affected by the Doppler shifted transitions at 169.3-keV in ^{13}C produced by the reaction between ^{6}Li and ^{12}C backing materials.
(c) Doublets in ^{92}Mo.

The observed 12_1^- state in Fig. 6 can be also roughly explained by JUN45 shell-model calculation with a quite difference configuration (see Table II) which is a mixture between $\pi((p_{3/2})^3,(f_{5/2})^6,(p_{1/2})^2,(g_{9/2})^3)$ and $\pi((p_{3/2})^4,(f_{5/2})^5,(p_{1/2})^2,(g_{9/2})^3)$. Therefore, the experimental observed 2064-keV transition connecting 12_1^- and 11_1^- states could be viewed as a result of promoting proton across the $Z = 38$ sub-shell gap. It should be mentioned that a 300-keV overestimation is seen for 12_1^- by JUN45 calculation, and it is not surprising that the overestimation becomes more significantly for higher-lying states such as 13_1^- and 14_1^- as shown in Fig. 6, since the $N = 50$ across shell excitation could be also expected to contribute in this region.

At the same time, a newly measured state at 6977 keV is tentatively assigned to be (12_2^-) state since it directly decays towards 11_1^- state by a high-energy (2490 keV) transition. Another two levels at 8380 and 9275 keV, tentatively assigned as (14^-) states, are also observed for the first time which decay to (13_1^-) via 1718 and 2614 keV transitions, respectively.

Being similar to the situation in positive band as mentioned in the previous subsection, the JUN45 calculation hardly reproduces all these negative states higher than 6.5 MeV. As shown in Table II, the JUN45 calculation also includes the second 12^- and 13^- states, which are more fragmented in their configurations. Meanwhile, these states are predicted to be 600–800 keV higher than the yrast one, thus no experimental levels can match them within a 500 keV energy difference. Thus, it may be another indication that a larger model space is necessary to understand the higher-lying negative-parity states.

C. E1 strength

The $E1$ transitions are strictly forbidden within the JUN45 model space, since there are no orbitals which can satisfy $\Delta l = \Delta j = 1$ relationship for $E1$ operator. This is also consistent with the experimental results that all the $E1$ transitions in ^{92}Mo are highly hindered, leading to a rare communication between the aforementioned positive and negative bands, as well as the fact that the lowest 5^- state becomes an isomeric state. The similar situation can be also found in ^{94}Ru, ^{96}Pd and ^{98}Cd.

Meanwhile, even though very weak, the strength of such highly-suppressed $E1$ transition could be very sensitive to (at least) two sources: (1) the interplay between the $f_{5/2}$ and $p_{3/2}$ orbits and the high-lying one such as $g_{7/2}$ and $d_{5/2}$ above the $N = Z$ =50 shell, and (2) the transition of nucleon between the $g_{9/2}$ orbit and the deep-lying $f_{7/2}$ orbit below the $N = Z$ =28 shell.

From the experimental side, in this work a new $E1$ transition at 1012 keV is observed which connects the first 7^- state and the first 6^+ state. Another $E1$ transition at 1491 keV is also observed unambiguously for the first time, connecting 9_1^- with 8_1^+ states as shown in Fig. 1.

From the theoretical side, the $E1$ strengths are investigated by using JJGLEM calculation which includes the proton $f_{7/2}$ orbit below the $Z = 28$ shell. With the limitation that only one proton can be excited from the $f_{7/2}$ orbit, the weak $E1$ transitions between the negative states and the positive states can be predicted as list in Table III in comparison with the experimental result. Even though the inclusion of $Z = 28$ proton core-breaking contribution could be helpful, the B($E1$)s are still considerably underestimated by the current calculations. The $E1$ transition from the first 5^- state to the state 4^+ is taken as an example. The experimental B($E1$) is obtained from the measured lifetime of the 5^- state [26], giving rise to a maximum limitation: $1.48(4)\times10^{-5}$ W.u. when assuming a pure $E1$ component. The calculated B($E1$) for the same transition is 1.84×10^{-6} W.u., being ≈8 lower than the experimental limitation. The missing strengths could be attributed to Z = N = 50 core-excitation which has been qualitatively studied in ^{94}Ru (see Ref. [6]).

On the other side, the JJGLEM also predicts a branching ratio of 12.7% between 627-keV ($9_1^- \rightarrow 7_1^-$) and 1491-keV ($9_1^- \rightarrow 8_1^+$) transitions. Meanwhile, the measured branching ratio is 3.5(2)%. The overestimation of the branching ratio by a factor of ≈4 also indicates that more efforts on the theoretical side are deserved in order to fully understand the highly hindered $E1$ transition in this region.

Before ending the discussion part, we want to also comment on the level scheme predicted by JJGLEM model as shown in Fig. 6. For both positive and negative bands, the JJGLEM can reasonably reproduce the low-lying states from 0^+ to 8^+ and 5^- to 11^-. Anyhow, the possible spurious components induced by center-of-mass when the model space includes both $f_{7/2}$ and $g_{9/2}$ orbits, seem not to totally destroy the prediction power of JJGLEM calculation. It is certainly that more comparisons with the experimental data are essential to verify the feasibility of this model space.

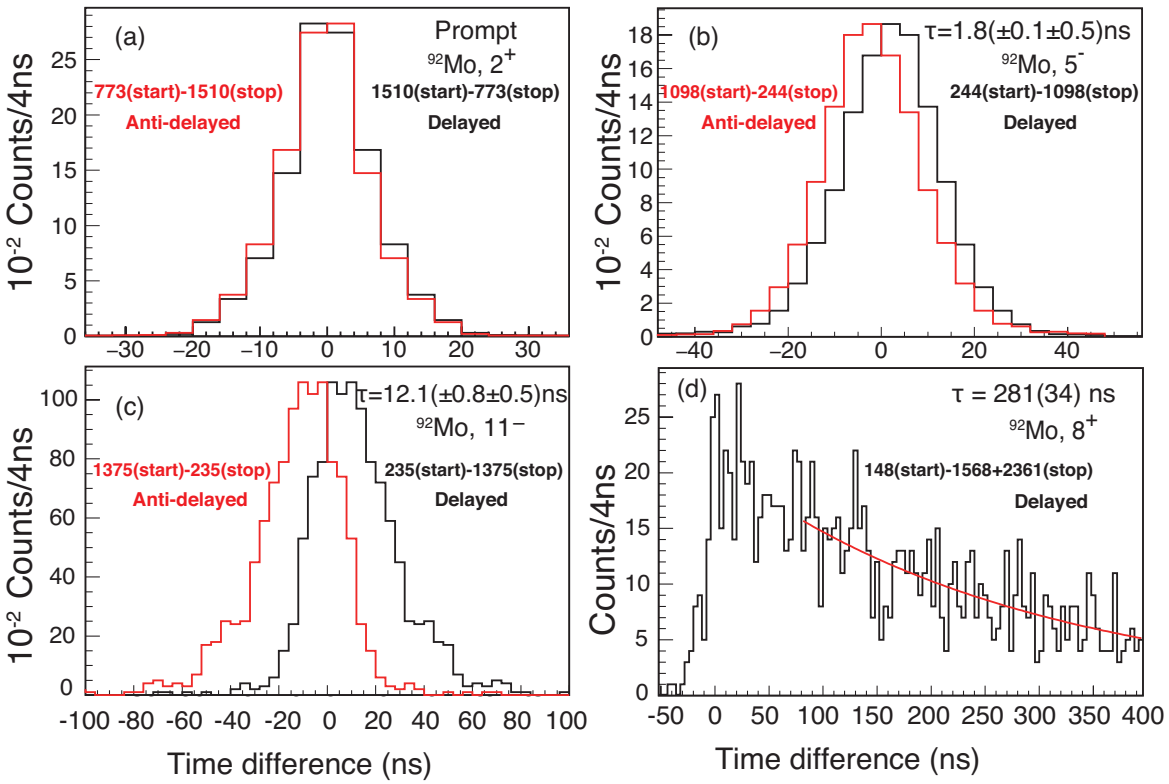

FIG. 5. Gamma-ray time difference spectra. Delayed and anti-delayed time distributions for 773-1510, 1098-244, and 1375-235 keV coincidences are shown in panels (a), (b), and (c), respectively. (d) The exponential fit of the sum of delayed time distributions of 148-1568 and 148-2361 keV coincidences.

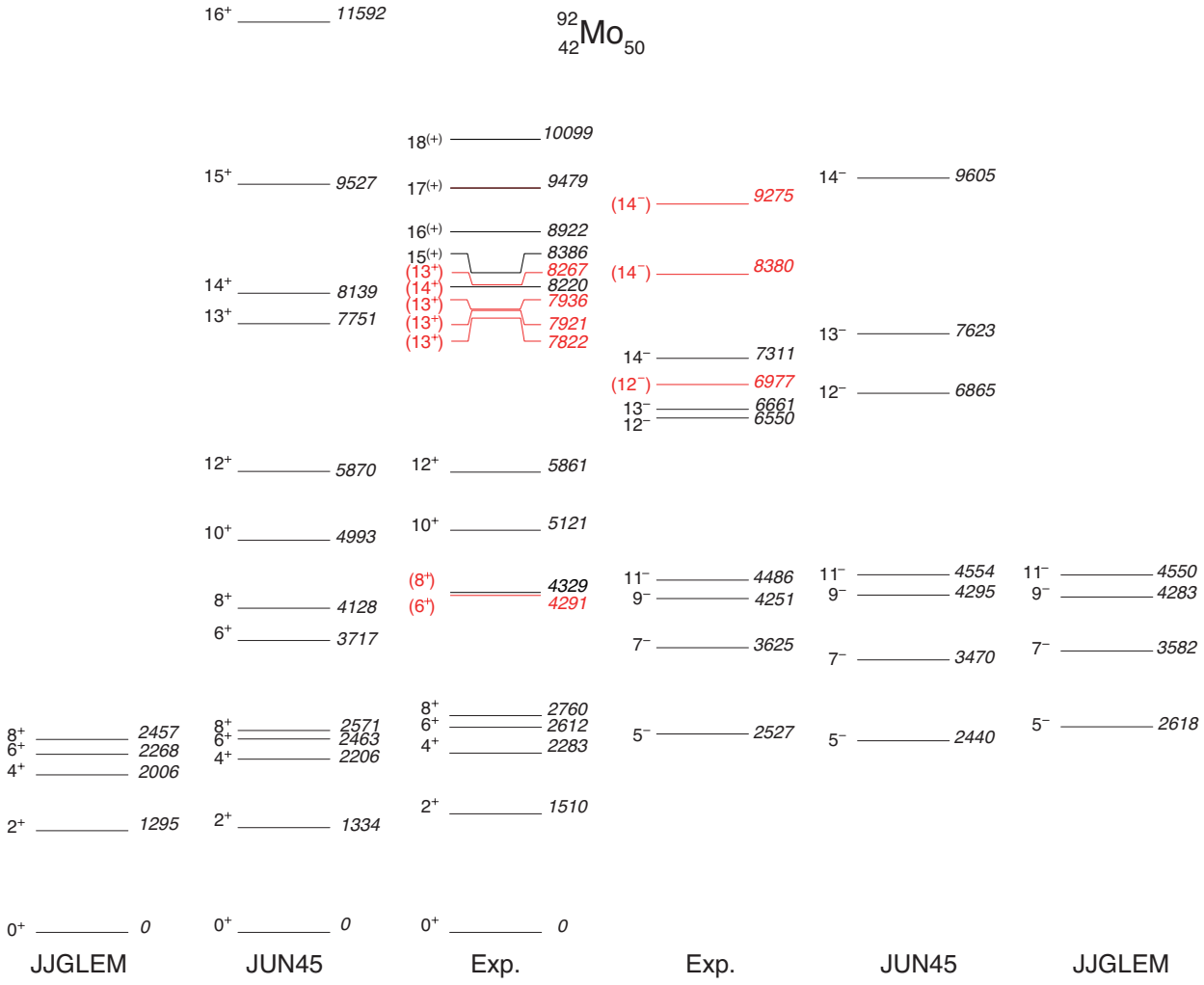

FIG. 6. Comparison between the observed excitation energies and the shell-model calculations for ^{92}Mo. The excitation energies are shown in keV unit.

TABLE II. Summary of JUN45 calculation. Only main partitions ($\geq$ 10%) of wave functions are shown in the form of $P = [\pi(p(1), p(2), p(3), p(4))]$, where $p(i)$ represents the number of protons occupying the $p_{3/2}$, $f_{5/2}$, $p_{1/2}$, and $g_{9/2}$ orbits. Not all the listed levels are included in the Fig. 6.

J ($\hbar$)	Energy (Jun45) (keV)	Wave function π	Partitions (%)
0^+	0	π(4,6,2,2)	44.95
		π(4,6,0,4)	21.10
		π(2,6,2,4)	16.21
2^+	1334	π(4,6,2,2)	57.83
		π(4,6,0,4)	14.44
		π(2,6,2,4)	11.93
4^+	2206	π(4,6,2,2)	57.90
		π(4,6,0,4)	15.61
		π(2,6,2,4)	11.43
6_1^+	2463	π(4,6,2,2)	59.93
		π(4,6,0,4)	14.58
		π(2,6,2,4)	11.43
6_2^+	3717	π(4,6,0,4)	70.61
		π(2,6,2,4)	14.53
8_1^+	2571	π(4,6,2,2)	59.39
		π(4,6,0,4)	15.62
		π(2,6,2,4)	11.55
8_2^+	4128	π(4,6,0,4)	51.26
		π(4,6,2,2)	20.27
10^+	4993	π(4,6,0,4)	73.53
		π(2,6,2,4)	14.32
12^+	5870	π(4,6,0,4)	76.28
		π(2,6,2,4)	14.25
13_1^+	7751	π(3,6,1,4)	80.44
13_2^+	8453	π(4,5,1,4)	87.10
14_1^+	8139	π(3,6,1,4)	77.07
14_2^+	8946	π(4,5,1,4)	85.70
5_1^-	2440	π(4,6,1,3)	77.80
		π(2,6,1,5)	12.74
7^-	3470	π(4,6,1,3)	83.25
9^-	4295	π(4,6,1,3)	81.88
11^-	4554	π(4,6,1,3)	86.61
12_1^-	6865	π(3,6,2,3)	58.86
		π(4,5,2,3)	22.13
12_2^-	7481	π(4,5,2,3)	44.13
		π(3,6,0,5)	17.20
		π(3,6,2,3)	14.72
13_1^-	7623	π(4,5,2,3)	64.12
		π(4,5,0,5)	18.08
		π(2,5,2,5)	10.19
13_2^-	8453	π(4,5,0,5)	34.26
		π(3,6,0,5)	28.22
		π(4,5,2,3)	16.13
14^-	9605	π(3,6,0,5)	74.31

TABLE III. Experimental reduced transition probabilities for the observed $E1$ γ-ray transitions as deduced from the branching ratios (this work), internal-conversion coefficient, and the lifetimes [26] of the initial states in comparison with the results of the shell model calculation JJGLEM (see text). Uncertainties are given in parentheses.

Eγ (keV)	$J_i^\pi \rightarrow J_f^\pi$	B(E1)^{exp} (W.u.)	B(E1)^{JJGLEM} (W.u.)
244	$5_1^- \rightarrow 4^+$	$1.48(4)\times10^{-5}$	1.84×10^{-6}
85	$6_1^+ \rightarrow 5_1^-$	$>3.83(16)\times10^{-5}$	1.82×10^{-6}

V. CONCLUSIONS

The experiment of ^{89}Y(^{6}Li,3n)^{92}Mo was performed at the tandem of INFN-Legnaro National Laboratory in Italy. With γ rays detected by GALILEO array, level scheme of ^{92}Mo has been revisited and enriched considerably in the current work. The meta-stable states in ^{92}Mo with lifetime longer than few nano-seconds are also remeasured in this experiment. Via the comparison between the experimental results and JUN45 shell-model calculation, the several high-energy transitions ($\approx$ 2000 keV) directly feeding the 12^+ or 11^- states are tentatively assigned to $Z = 38$ across shell excitation or $Z = N = 50$ core excitation. The $E1$ strengths of transitions between the two lowing-lying positive and the negative bands show a fair agreement with JJGLEM calculation which enlarges the model space to $f_{7/2}$ orbit, which means that the proton $Z = 28$ core-breaking effect could be one of the contribution to the $E1$ transitions.

ACKNOWLEDGMENTS

We are grateful to the INFN-LNL staff for providing stable ^{6}Li beam throughout the experiment. This work is supported by the National Nature Science Foundation of China under Grant Nos. 11975040, U2167204 and U1832130. Z. Huang is supported by the China Scholarship Council (CSC). The Brazilian authors acknowledge partial financial support from CNPq, FAPERJ, and CAPES and from INCT-FNA (Instituto Nacional de Ciência e Tecnologia- Física Nuclear e Aplicações), research project 464898/2014-5. P. R. John is supported by BMBF project No. 05P19RDFN1. M. Siciliano is supported by U.S. Department of Energy, Office of Science, Office of Nuclear Physics, under the Contract No. DE-AC02-06CH11357. S. P. Hu is supported by Guangdong Key Research And Development Program 2020B040420005, Shenzhen Universities Stable Support Program 20200813080048001, and Foundation of National Laboratory of Heavy Ion Accelerator of Lanzhou 20200602SZU.

[1] E. Caurier, *et al.*, Rev. Mod. Phys. **77**, 427 (2005).
[2] H. Mach, *et al.*, Phys. Rev. C. **95**, 014313 (2017).
[3] B. Das, *et al.*, Phys. Rev. C. **105**, L031304 (2022).
[4] R.M. Pérez-Vidal, *et al.*, Phys. Rev. Lett. **129**, 112501 (2022).
[5] K. Muto, *et al.*, Phys. Lett. B **135** (5-6), 349-352 (1984).
[6] F. G. Moradi, *et al.*, Phys. Rev. C. **89**, 014301 (2014).
[7] M. Palacz, *et al.*, Phys. Rev. C. **86**, 014318 (2012).
[8] A. Blazhev, *et al.*, Phys. Rev. C. **69**, 064304 (2004).
[9] J. M. Jaklevic, *et al.*, Phys. Lett. **29B**, 179 (1969).
[10] T. Numao, *et al.*, Nucl. Phys. A **305**, 163-166 (1978).
[11] C. M. Lederer, *et al.*, Nucl. Phys. A **169**, 449-488 (1971).
[12] P. Singh, R. G. Pillay, J. A. Sheikh, and H. E. Devare, Phys. Rev. C **45**, 2161 (1992).
[13] S. Cochavi, *et al.*, Phys. Rev. C **3**, 1352 (1971).
[14] S. S. Ghugre and S. K. Datta, Phys. Rev. C **52**, 1881 (1995).
[15] N. S. Pattabiraman *et al.*, Phys. Rev. C **65**, 044324 (2002).
[16] A. Goasduff, D. Mengoni, F. Recchia, J. J. Valiente-Dobon, *et al.*, Nucl. Instrum. Methods. Phys. Res. A 1015, 165753 (2021).
[17] D. Testov *et al.*, Eur. Phys. J. A **55**, 47 (2019).
[18] S. P. Hu *et al.*, Nucl. Instrum. Methods in Phys. Res. A **914**, 64 (2019).
[19] J. T. Li *et al.*, Nucl. Sci. Tech. **31**, 49 (2020).
[20] J. Gutleber, S. Murray, and L. Orsini, Computer Physics Communications **153**, 155-163 (2003).
[21] D. Barientos, *et al.*, Nuclear Science **62**, 3134 (2015).
[22] M. Rocchini, Ph.D. Thesis, Universit*à* degli studi di Firenze, 2017.
[23] T. Fukuchi *et al.*, Eur. Phys. J. A **24**, 249-257 (2005).
[24] A. Balanda, *et al.*, Acta Physica Polonica Series B **9**(11):995-1001 (1978).
[25] L. I. Govor *et al.*, Phys. At. Nucl. **73**, 1289-1299 (2010).
[26] Coral M. Baglin, NDS **113**, 2187 (2012).
[27] M. Piiparinen *et al.*, Nuclear Physics A **605**, 191 (1996).
[28] J. M. Régis, G. Pascovici, J. Jolie and M. Rudigier, Nucl. Instrum. Methods in Phys. Res. A **897**, 83-92(2010).
[29] J. M. Régis, M. Dannhoff and J. Jolie, Nucl. Instrum. Methods in Phys. Res. A, **622** 38–46(2018).
[30] N. Shimizu, *et al.*, Comp. Phys. Comm. **244**, 372 (2019).
[31] M. Honma, *et al.*, Phys. Rev. C **80**, 064323 (2009).
[32] A. F. Lisetskiy, *et al.*, Phys. Rev. C **70**, 044314 (2004).
[33] H. Mach, *et al.*, Phys. Rev. C **41**, 226-242 (1990).
[34] A. Hosaka, K. I. Kubo and H. Toki, Nucl. Phys. A **444**, 76-92 (1985).
[35] Z. Huang *et al.*, Eur. Phys. J. A **57**, 137 (2021).
[36] J. P. Elliott and T. H. R. Skyrme. Proc. R. Soc. Lond. A **232**, 561-566 (1955).
[37] P. F. Casten, Phys. Lett. B **152**, 145 (1985).
[38] S. Y. Jin, *et al.*, Phys. Rev. C **104**, 024302 (2021).